Electron microscopy and positron annihilation study of CdSe nanoclusters embedded in MgO

van Huis, M.A.; van Veen, A.; Schut, H.; Eijt, S.W.H.; Kooi, B.J.; de Hosson, J.T.M.

Published in:
Nuclear Instruments & Methods in Physics Research Section B-Beam Interactions with Materials and Atoms

DOI:
10.1016/j.nimb.2004.01.008

Publication date:
2004

Available online at www.sciencedirect.com
SCIENCE DIRECT®
ELSEVIER
Nuclear Instruments and Methods in Physics Research B 218 (2004) 410–415
NIM B
Beam Interactions with Materials & Atoms
www.elsevier.com/locate/nimb

Electron microscopy and positron annihilation study of CdSe nanoclusters embedded in MgO

M.A. van Huis [a,*], A. van Veen [a], H. Schut [a], S.W.H. Eijt [a], B.J. Kooi [b], J.Th.M. De Hosson [b]

[a] *Interfaculty Reactor Institute, Delft University of Technology, Mekelweg 15, Delft 2629 JB, The Netherlands*
[b] *Materials Science Center, University of Groningen, Groningen, The Netherlands*

Abstract

CdSe nanoclusters are created in MgO by means of co-implantation of 280 keV, 1×10^{16} Cd ions cm^{-2} and 210 keV, 1×10^{16} Se ions cm^{-2} in single crystals of MgO(0 0 1) and subsequent thermal annealing at a temperature of 1300 K. The structural properties and the orientation relationship between the CdSe and the MgO are investigated using cross-sectional transmission electron microscopy (XTEM). The crystal structure of the nanoclusters depends on their size. The smallest nanoclusters with a size below 5 nm have the cubic rocksalt crystal structure. The larger nanoclusters have a different (most likely the cubic sphalerite) crystal structure. The defect evolution in the sample after ion implantation and during thermal annealing is investigated using Doppler broadening positron beam analysis (PBA). The defect evolution in samples co-implanted with Cd and Se is compared to the defect evolution in samples implanted with only Cd or only Se ions.

1. Introduction

The optical, electronic, magnetic and structural properties of nanoclusters change as a function of size [1], offering the opportunity to change material properties by changing the size of the clusters. In particular semiconductor nanoclusters are interesting because their electronic properties change already below quite large sizes of ~10 nm, which is considerably larger than for metal nanoclusters whose electronic properties only change below a few nanometer. CdSe nanoclusters display a few very interesting size effects: structural change transformations (the rocksalt, sphalerite and wurtzite CdSe crystal structure can occur) [2,3], and widening of the band gap with decreasing nanocluster size. The band gap of CdSe nanoclusters with a size of 2 nm is 2.5 eV, considerably larger than the band gap of bulk CdSe, 1.8 eV [4,5]. Ion implantation provides a feasible method to create embedded CdSe nanoclusters by sequential Cd and Se ion implantation and subsequent thermal annealing. The advantage of embedding the nanoclusters in an insulator such as MgO is that the nanoclusters are electronically passivated in the insulator material (MgO has a band gap of 7.8 eV) while MgO is optically transparent so that optical properties such as optical absorption spectroscopy and photoluminescence can still be investigated. CdSe nanoclusters

* Corresponding author. Tel.: +31-15-278-1612; fax: +31-15-278-6422.
E-mail address: vanhuis@iri.tudelft.nl (M.A. van Huis).

0168-583X/$ - see front matter © 2004 Elsevier B.V. All rights reserved.
doi:10.1016/j.nimb.2004.01.008

were previously successfully created in Al_2O_3 and SiO_2 [6,7]. The structural properties of CdSe nanoclusters embedded in MgO are discussed in an earlier work [3]. Nanoclusters smaller than 5 nm adopt the rocksalt crystal structure while larger nanoclusters adopt either the cubic sphalerite or the hexagonal wurtzite crystal structure. In the present work, the focus is on the defect evolution during the ion implantation and the subsequent thermal treatment. The presence of CdSe nanoclusters is investigated by means of transmission electron microscopy. Doppler broadening positron beam analysis (PBA) is employed to monitor the defect evolution in the sample. Positrons are probes that are very sensitive for detection of vacancy-type defects, which are always created during ion implantation.

2. Experimental

Single crystals of MgO(0 0 1) with sizes of $10\times10\times1$ mm^3 were implanted with either 1×10^{16} Cd ions cm^{-2} at an energy of 280 keV, or with 1×10^{16} Se ions cm^{-2} at an energy of 210 keV, or with both ions to the same doses and energies. These energies were chosen so that the depth distributions of the implanted Cd and Se ions overlap as much as possible. The sample surface was perpendicular to the incoming beam within an angle of a few degrees. Next, the samples were annealed in ambient air for 30 min at incrementing temperatures, from room temperature to 1500 K in steps of 200 K. Ambient air was used in order to maintain the stoichiometry of MgO. The electron microscopy results discussed below, show that no oxidation of Cd or Se occurred. After every annealing step, the samples were cooled down and measured with Doppler broadening positron beam analysis (PBA) [8]. Positrons that are implanted in a material annihilate with electrons, giving two γ quanta per annihilation with an energy of 511 keV each. The energy of the photons is measured using an energy-sensitive detector and accumulated in a multi-channel analyser. The non-zero momentum of the electrons leads to a Doppler broadening of the 511 keV annihilation peak. The so-called S (shape) parameter is derived from the 511 keV peak and indicates the contribution of valence and conduction electrons to the annihilation spectrum [8]. Ion implantation leads to the formation of vacancies where positrons are effectively trapped and mainly annihilate with valence electrons. Hence, the S parameter is a very sensitive indicator of ion implantation damage. PBA is also a depth-sensitive technique; the probe depth in the sample can be varied by varying the implantation energy of the positron beam. In this work, a mono-energetic positron beam with a variable energy of 0–30 keV was used, allowing detection up to 2 μm in depth. The sample implanted with both Cd and Se ions was analysed with cross-sectional transmission electron microscopy (XTEM) after the 1300 K annealing step. The microscope was a JEOL 4000 EX/II operating at 400 kV with a point-to-point resolution of 0.17 nm. The specimen preparation is discussed elsewhere [9].

3. Results and discussion

3.1. Ion implantation simulations

The depth distribution of the implanted ions and the ion implantation damage can be simulated using the SRIM 2000 code [10]. A threshold displacement energy of 55 eV was used for both the Mg and the O atoms [11]. Fig. 1 shows the concentration of implanted ion species as a function of depth. As can be seen from the figure and the data given in Table 1, the range of both ions is approximately 83 nm and the straggling of the Se ions is slightly larger than the straggling of the Cd ions. Despite these small deviations, the predicted ion depth distributions overlap to a large extent. The concentration of Cd or Se ions in the peak of the distributions is approximately 1.6 at.%. If both Cd and Se are implanted, the concentration of "CdSe" is 1.6 mol.% (molecule CdSe per molecule MgO). As Cd and Se both have a low melting point and CdSe a high melting point (see Table 1) it is likely that Cd and Se will agglomerate to create a more stable phase. It is assumed that the profiles will still overlap to a

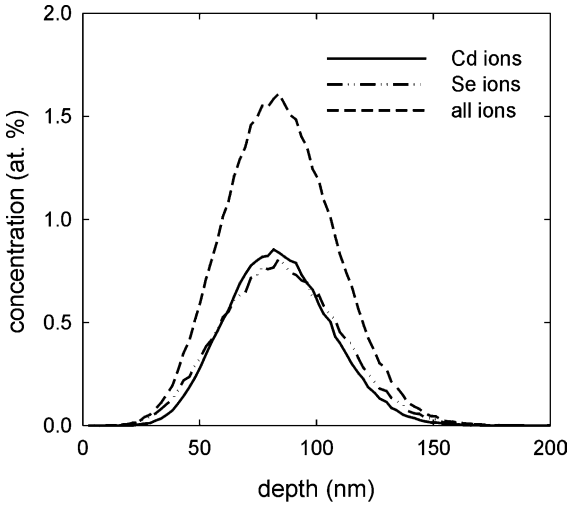

Fig. 1. Atomic concentration of implanted Cd and Se atoms as a function of depth, calculated using the SRIM ion implantation code [10].

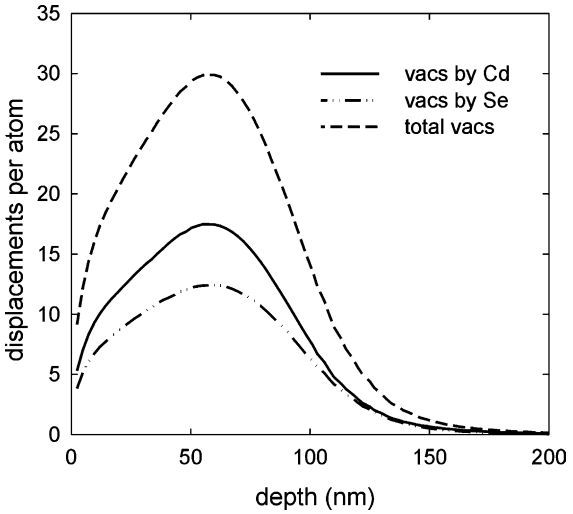

Fig. 2. Number of displacements per target atom in MgO as a function of depth, created by ion implantation of 1×10^{16} Cd ions cm^{-2} or 1×10^{16} 210 keV Se ions cm^{-2}, or both. These distributions are calculated using the SRIM ion implantation code [10].

Table 1
Ion implantation parameters and bulk properties of Cd, Se and CdSe

Material	Cd	Se	CdSe
Ion energy (keV)	280	210	–
Implanted dose (cm^{-2})	1×10^{16}	1×10^{16}	$\sim10^{16}$
Range (nm)	82	83	83
Concentration in at.%	1.7	1.5	3.2
Displacements per atom (dpa)	17	12	30
Melting temperature (K)	594	490	1350

The impurity concentrations and the displacements per ion are valid for the peak of the depth distribution and have been calculated with the SRIM code [10]. Melting temperatures are obtained from [13].

large extent after thermal annealing. The XTEM results discussed below indicate that the implanted ion species do not significantly dissolve or diffuse away into the bulk MgO up to an annealing temperature of 1300 K. Fig. 2 shows the damage depth distributions for all three samples, indicated by the number of displacements per target atom (dpa). The dpa level can reach a value of 30 in the peak of the damage distribution when both Cd and Se are implanted. Of these 30 dpa, most are caused by the Cd ion implantation (17 dpa) while the Se ions contribute less (12 dpa).

3.2. XTEM results

The TEM analysis was only performed on the sample implanted with both 280 keV Cd and 210 keV Se ions to a dose of 1×10^{16} ions cm^{-2} each, after annealing at 1300 K. Fig. 3 is a high-resolution TEM image displaying two CdSe phases that occur in MgO. At the top of the figure, there are small rocksalt (fcc-type) CdSe nanoclusters that can be identified by their moiré fringes [3]. They are in a cube-on-cube orientation relationship with the MgO. At the bottom, a large CdSe nanocluster is present that has either the sphalerite (cubic) or the wurtzite (hexagonal) crystal structure. The difference between the sphalerite and wurtzite crystal structure is small because the interplanar spacing of the sphalerite (1 1 1) planes and the wurtzite (0 0 0 1) planes is very similar. However, when comparing the experimental TEM observations of large CdSe clusters with preliminary HRTEM simulations, there are strong indications that the large CdSe nanoclusters have the sphalerite crystal structure.

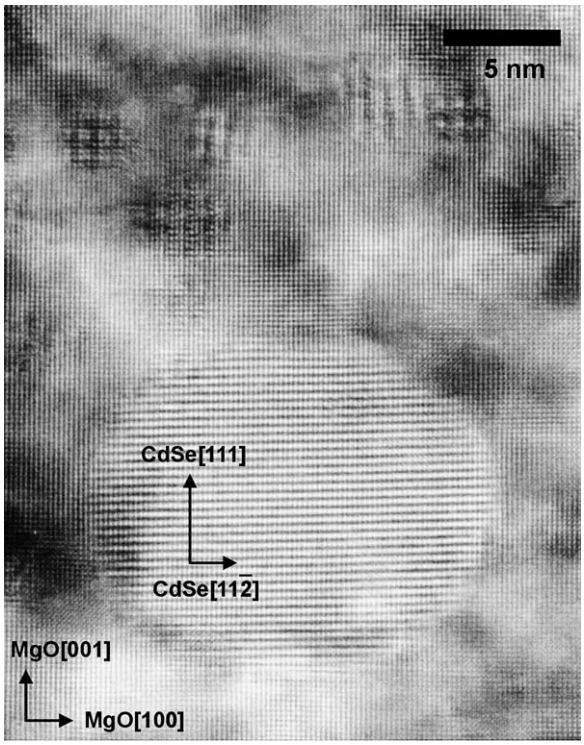

Fig. 3. High-resolution TEM image showing a large CdSe nanocluster having either the sphalerite (fcc) or wurtzite (hcp) structure. The CdSe crystal axes are indicated for the case of the sphalerite structure. At the top of the image, a number of small nanoclusters with the rocksalt crystal structure can be observed by their moiré fringes.

3.3. PBA results

Fig. 4 shows the *S* parameter (indicator of open volume defects) as a function of the positron implantation energy. Of course, the positron energy is related to the probe depth in the samples. Unfortunately, the depth resolution of the PBA technique is limited by the positron implantation profile and positron diffusion processes and we prefer to plot the *S* parameter as a function of positron energy rather than as a function of depth in the sample. However, the average positron implantation depth is indicated at the top of the figure. The *S* parameter curves were recorded after ion implantation and after every annealing step. Fig. 4 displays the defects evolution of the MgO crystals implanted with only Cd ions (A), only Se ions (B), and sequentially implanted with both ions (C). At large positron implantation depths, the positrons sense the MgO bulk (which has an *S* parameter of 0.468). After ion implantation, there is an increase in the *S* parameter compared to defect-free MgO at a positron implantation energy of 1–2 keV. During annealing at 500–1100 K the *S* parameter steadily increases in the ion implantation range (at a depth of 20–150 nm) indicating that vacancy-type defects are agglomerating and forming vacancy clusters, possibly even nanovoids. Voids in the nanometer scale are easily created in MgO [12]. The ion implantation produces vacancy-interstitial pairs (Frenkel defects). Interstitials are very mobile in MgO and either recombine with the vacancies or migrate to the surface, leaving the vacancies behind. These vacancies agglomerate during thermal treatments. After annealing at 1100 K, the *S* parameter in the ion implantation range is at its maximum: the growth of voids has stopped. At higher annealing temperatures of 1300 and 1500 K, the *S* parameter decreases again as the voids shrink and finally

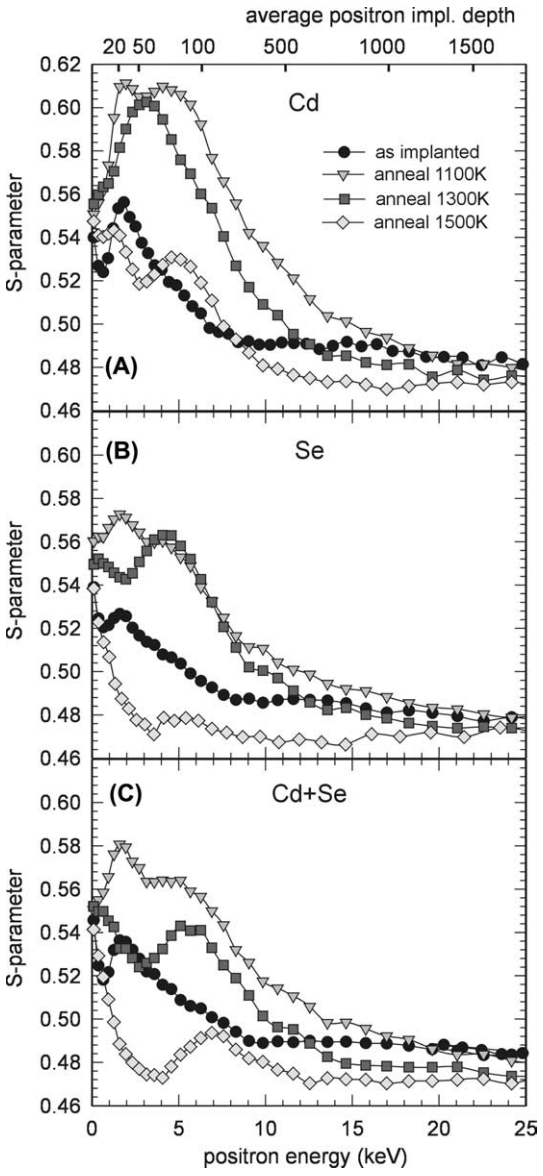

Fig. 4. *S* parameter as a function of positron implantation energy. The average depth corresponding to the implantation energy is indicated at the top of the graph. Displayed are the curves after ion implantation and after various annealing steps, for MgO implanted with (A) only Cd ions, (B) only Se ions and (C) implanted with both Cd and Se ions.

dissociate. This behaviour is observed for all three implanted samples shown in Fig. 4.

There are large differences between the samples as well. The *S* parameter of the sample implanted with only Cd ions (Fig 4(A)) reaches very high values of 0.61 in the ion implantation range. This value is much higher than the value of the *S* parameter in the sample implanted with only Se ions (Fig. 4(B)) and the sample implanted with both Cd and Se ions (Fig. 4(C)) where the *S* parameter remains below a value of 0.58. Considering Table 1, the damage in the MgO:CdSe sample is considerably higher (30 dpa) than the damage in the MgO:Cd sample (17 dpa) so the high *S* parameter in the MgO:Cd case cannot be explained by the presence of more or larger vacancy-type defects. Let us consider Fig. 4(A). After annealing at 1100 K, there are two peaks in the *S* parameter. The first peak is the main damage peak, which is located somewhat shallower in depth than the ion range (compare Figs. 1 and 2). The second peak is caused by damage created by ions that undergo channelling. Amorphisation of MgO by means of ion implantation has – to our knowledge – never been reported in the literature and so the MgO remains crystalline. The channelling ions penetrate deeper into the MgO than the depths predicted by the SRIM simulation code, which assumes that the target material is amorphous. The ions that undergo channelling deposit damage behind the main ion range. Because of the very high sensitivity of positrons to vacancies and vacancy clusters, this damage band also appears in the *S* parameter plots. The "dip" in between these two peaks at a positron implantation energy of 3.0 keV corresponds to the main ion range. Here the ions have filled the vacancy-type defects. There are fewer vacancies for positrons to become trapped in, and consequently the *S* parameter is lower than in the surrounding defective material. After annealing at 1300 K, the vacancy clusters in the vacancy bands dissociate and the *S* parameter goes down. This can not only be observed for the MgO:Cd sample in Fig. 4(A), but for the other two samples as well. However, in the case of the MgO:Cd sample, the *S* parameter remains very high after annealing at 1300 K in the ion implantation range. The most plausible explanation is that the *S* parameter of Cd nanoclusters is unusually high. More dedicated positron annihilation experiments or calculations should be performed in order to test this hypothesis.

After annealing at a temperature of 1500 K, there is a very strong reduction in the S parameter for all three samples. It is remarkable that the deep vacancy band at a positron implantation energy of 6–7 keV still exhibits a high S parameter with respect to defect-free MgO, while the shallow vacancy band at a positron implantation energy of 1–2 keV has almost disappeared. Probably the shallow vacancy band is located so close to the surface that vacancies which dissociate from the vacancy clusters are trapped at the surface. At larger depths the surface is too far away to act as an efficient sink, and the probability to recombine with vacancy clusters is higher. Thus, the vacancy clusters in the deepest vacancy band are more stable.

4. Conclusions

MgO crystals have been implanted with only Cd ions, only Se ions and with both ions. In the sample implanted with both Cd and Se ions, CdSe nanoclusters were formed after thermal annealing at a temperature of 1300 K. These nanoclusters exhibit the rocksalt crystal structure at sizes below 5 nm, and a different (probably the sphalerite) crystal structure at larger sizes. When comparing the defect evolution as observed by means of Doppler broadening positron beam analysis for all samples, the S parameter is the highest for the case of the MgO:Cd sample, which is contrary to the expectations because the damage induced by Cd ion implantation alone is less than for the case of the MgO:CdSe sample. This can be explained if the Cd nanoclusters exhibit a very high S parameter.

References

[1] P.V. Kamat, D. Meisel (Eds.), Semiconductor Nanoclusters, Elsevier, New York, 1997.
[2] K. Jacobs, J. Wickham, A.P. Alivisatos, J. Phys. Chem. B Lett. 106 (2002) 3759.
[3] M.A. van Huis, A. van Veen, H. Schut, S.W.H. Eijt, B.J. Kooi, J.Th.M. De Hosson, Nucl. Instr. and Meth. B 216 (2004) 121.
[4] A.P. Alivisatos, Science 271 (1996) 933.
[5] A.P. Alivisatos, J. Phys. Chem. 100 (1996) 13226.
[6] C.W. White, J.D. Budai, S.P. Withrow, J.G. Zhu, E. Sonder, R.A. Zuhr, A. Meldrum, D.M. Hembree Jr., D.O. Henderson, S. Prawer, Nucl. Instr. and Meth. B 141 (1998) 228.
[7] C.W. White, A. Meldrum, J.D. Budai, S.P. Withrow, E. Sonder, R.A. Zuhr, D.M. Hembree Jr., M. Wu, D.O. Henderson, Nucl. Instr. and Meth. B 148 (1999) 991.
[8] A. van Veen, H. Schut, P.E. Mijnarends, in: P.G. Coleman (Ed.), Positron Beams and their Applications, World Scientific, Singapore, 2000, p. 191, Chapter 6.
[9] B.J. Kooi, A. van Veen, J.Th.M. De Hosson, H. Schut, A.V. Fedorov, F. Labohm, Appl. Phys. Lett. 76 (9) (2000) 1110.
[10] J.F. Ziegler, J.P. Biersack, U. Littmark, The Stopping and Range of Ions in Solids, Pergamon, New York, 1985.
[11] S.J. Zinkle, C. Kinoshita, J. Nucl. Mater. 251 (1997) 200.
[12] A. van Veen, M.A. van Huis, A.V. Fedorov, H. Schut, F. Labohm, B.J. Kooi, J.Th.M. De Hosson, Nucl. Instr. and Meth. B 191 (2002) 610.
[13] Handbook of Chemistry and Physics, 56th ed., CRC press, 1975.